Supplementary Material

Multi-stimuli-responsive DOX released from magnetosome for tumor synergistic theranostics

Ming-Fong Tsai[a,1], Yu-Lun Lo[a,1], Yuan-Chun Huang[a], Chun-Chieh Yu[b], Yi-Ting Wu[a], Chia-Hao Su[b,c*], and Li-Fang Wang[a,d*]

[a]*Department of Medicinal & Applied Chemistry, College of Life Sciences, Kaohsiung Medical University, Kaohsiung 807, Taiwan*

[b]*Institute for Translational Research in Biomedicine, Kaohsiung Chang Gung Memorial Hospital, Kaohsiung 833, Taiwan*

[c]*Department of Biomedical Imaging and Radiological Sciences, National Yang Ming University, Taipei 112, Taiwan*

[d]*Department of Medical Research, Kaohsiung Medical University Hospital, Kaohsiung 807, Taiwan*

[1]These authors contributed equally to this manuscript.

[*]**Corresponding authors**

Supplementary Figures

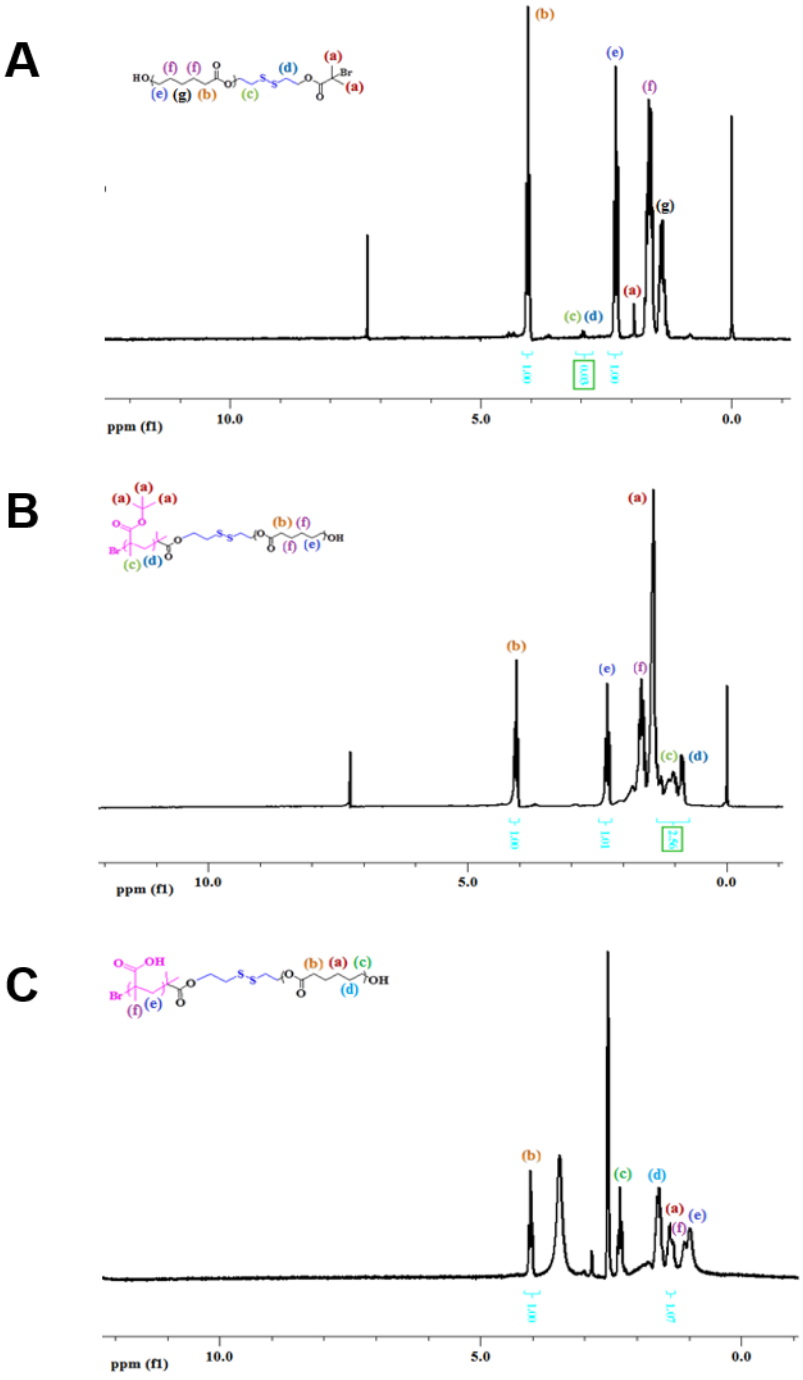

Supplementary Figure S1. Proton nuclear magnetic resonance spectra. (A) $(PCL)_{60}$-SS-Br in $CDCl_3$, **(B)** $(PCL)_{60}$-SS-(P*t*BMA)$_{60}$ in $CDCl_3$, and **(C)** $(PCL)_{60}$-SS-$(PMAA)_{60}$ in d_6-DMSO.

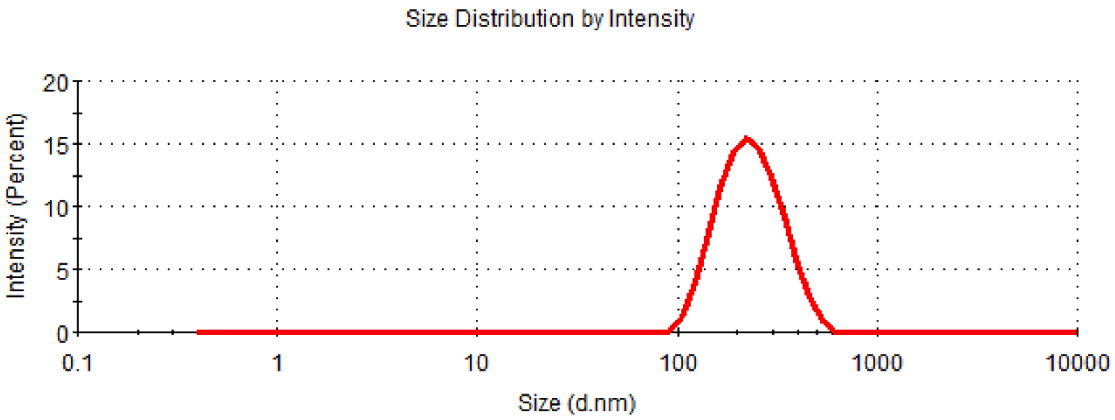

Supplementary Figure S2. Particle size measured by dynamic light scattering (DLS). The DLS diagram of PCL-SS-PMAA-formed polymersomes (PSPps) at pH 7.4.

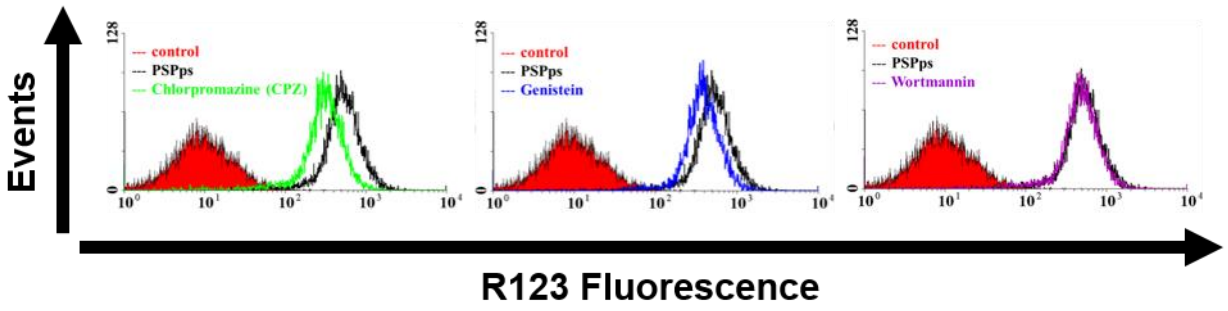

Supplementary Figure S3. **Internalization of PSPps into CRL-5802 cells.** Flow-cytometry diagrams of cells exposed to rhodamine 123 (R123)-linked PSPps at 250 µg·mL^{-1} for 4h of incubation after cells were pretreated with different chemical inhibitors: 10 µg·mL^{-1} chlorpromazine, 200 µM genistein and 50 nM wortmannin for 30 min.

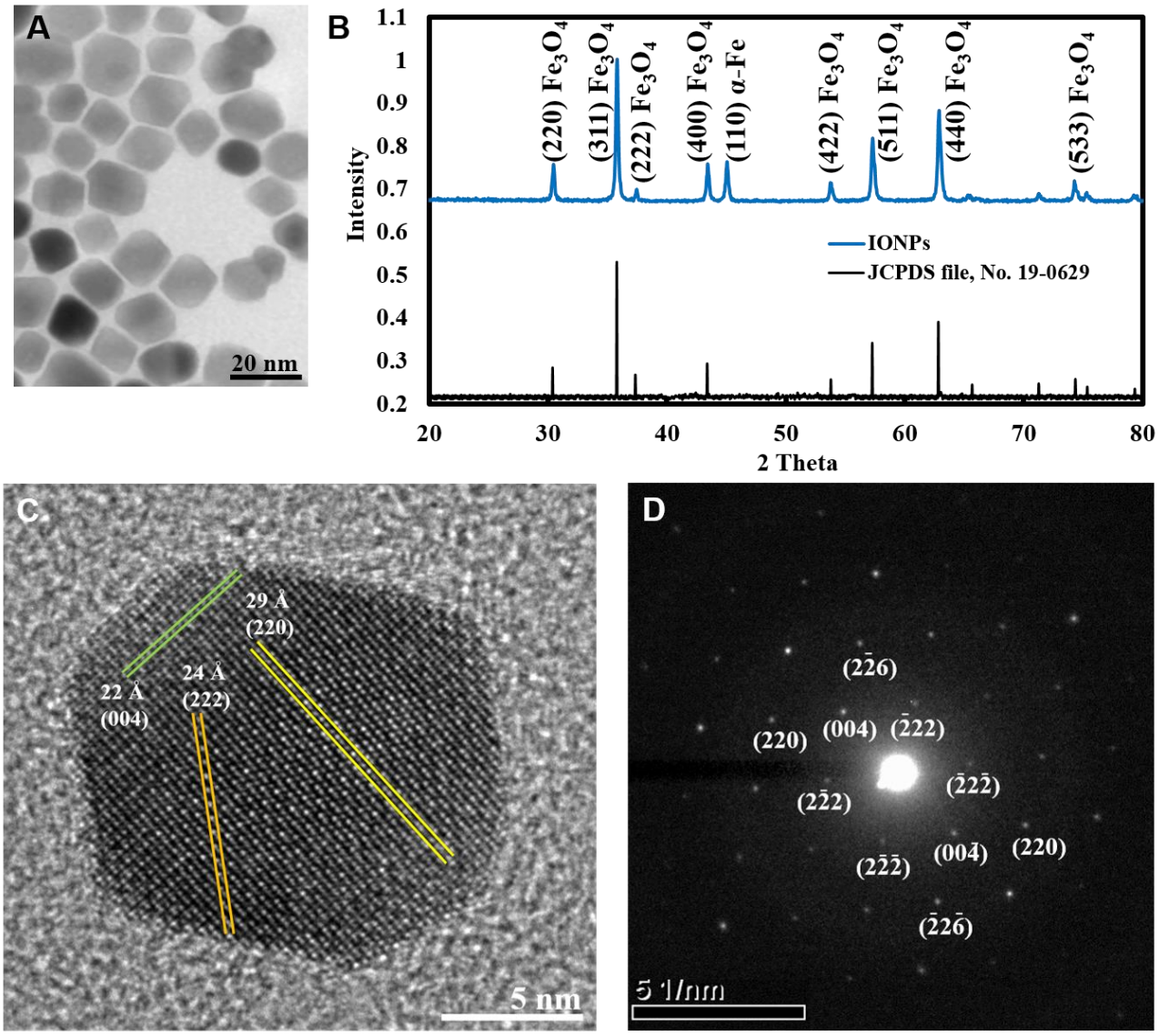

Supplementary Figure S4. Characteristic properties of truncated octahedral Fe_3O_4 nanoparticles (IONPs). (A) Transmission electron microscopy (TEM) image. **(B)** X-ray diffraction spectrum. **(C)** High-resolution TEM image. **(D)** Captured electron diffraction pattern.

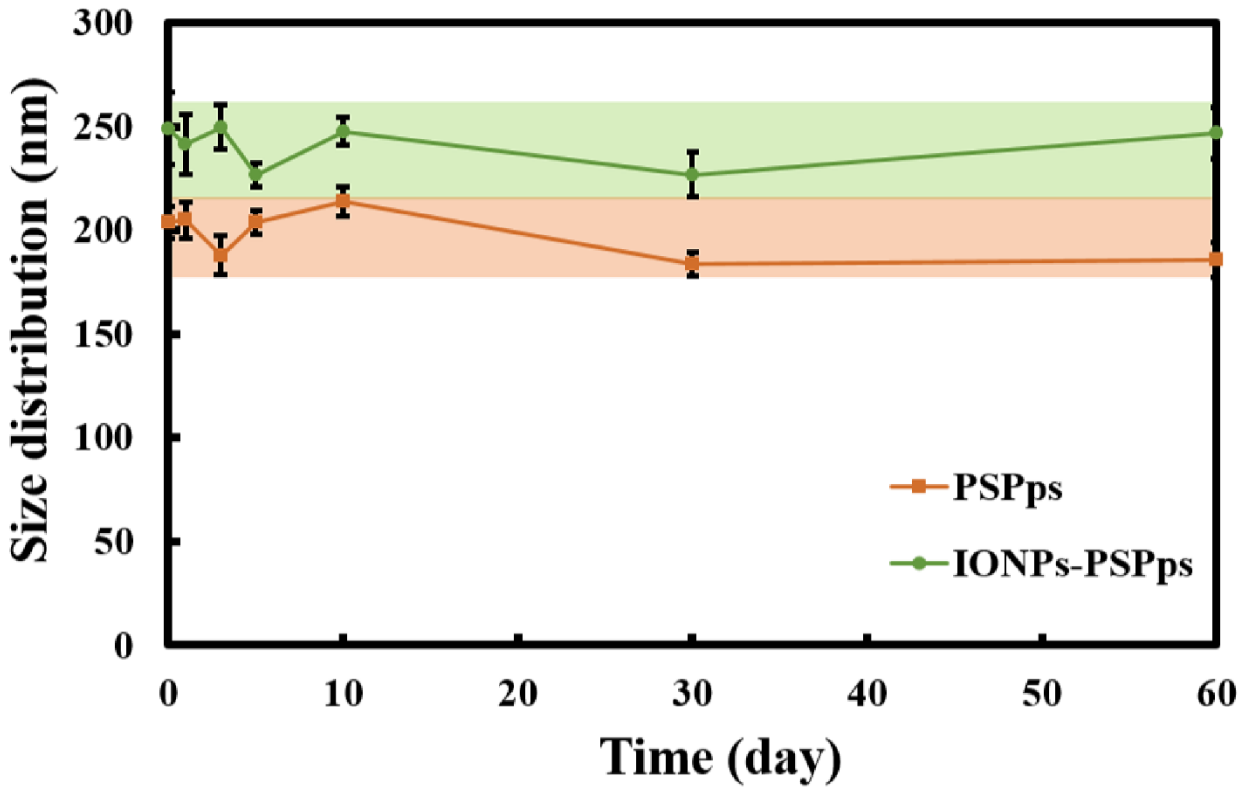

Supplementary Figure S5. Stability test. Size changes of PSPps and IONPs-PSPps NPs in PBS at pH 7.4 with time by DLS.

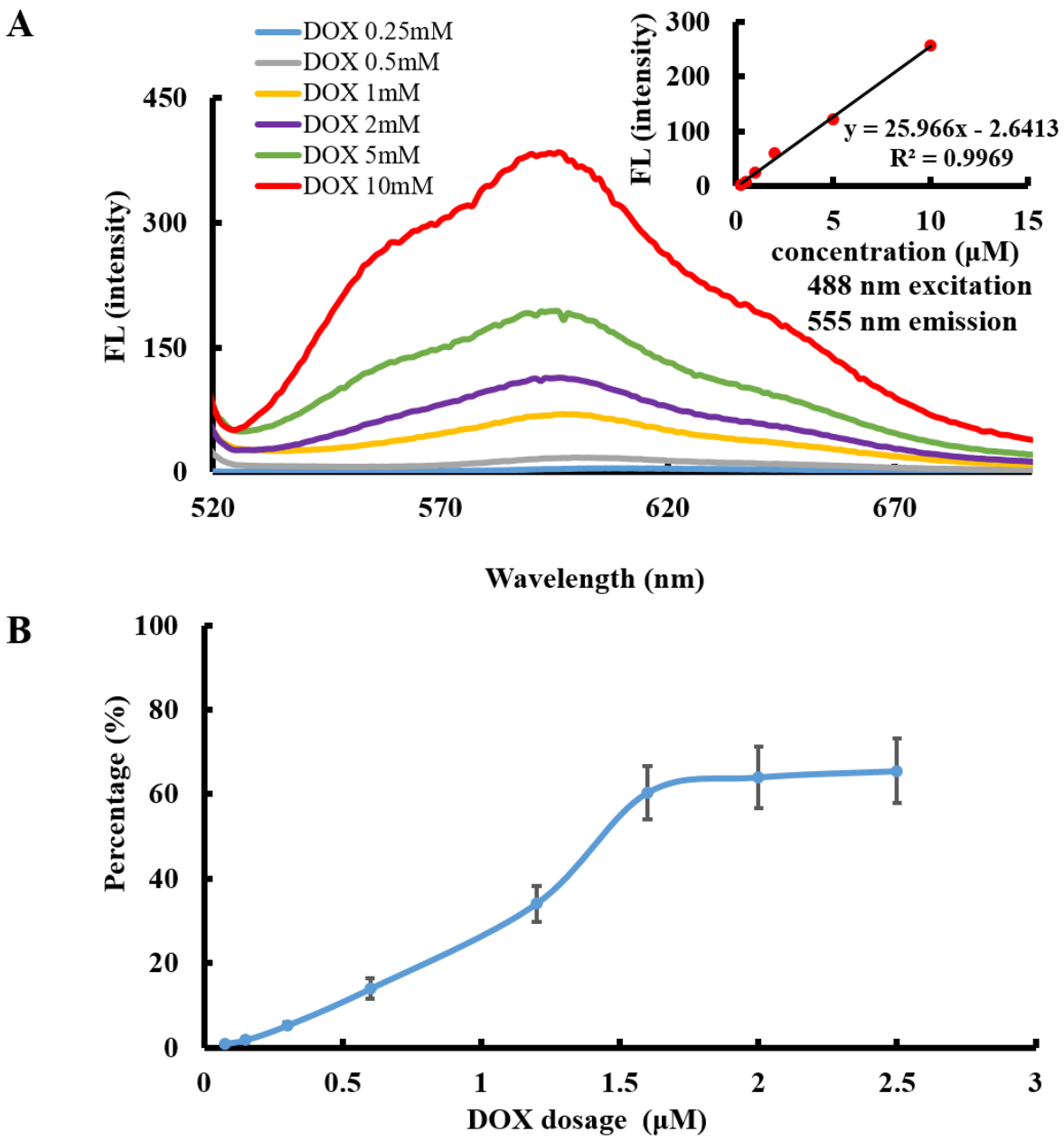

Supplementary Figure S6. Doxorubicin (DOX) encapsulation efficiency. (A) DOX calibration curve and **(B)** the percentage of DOX encapsulated with PSPps containing IONPs in the hydrophobic compartment for different amounts of DOX in feed.

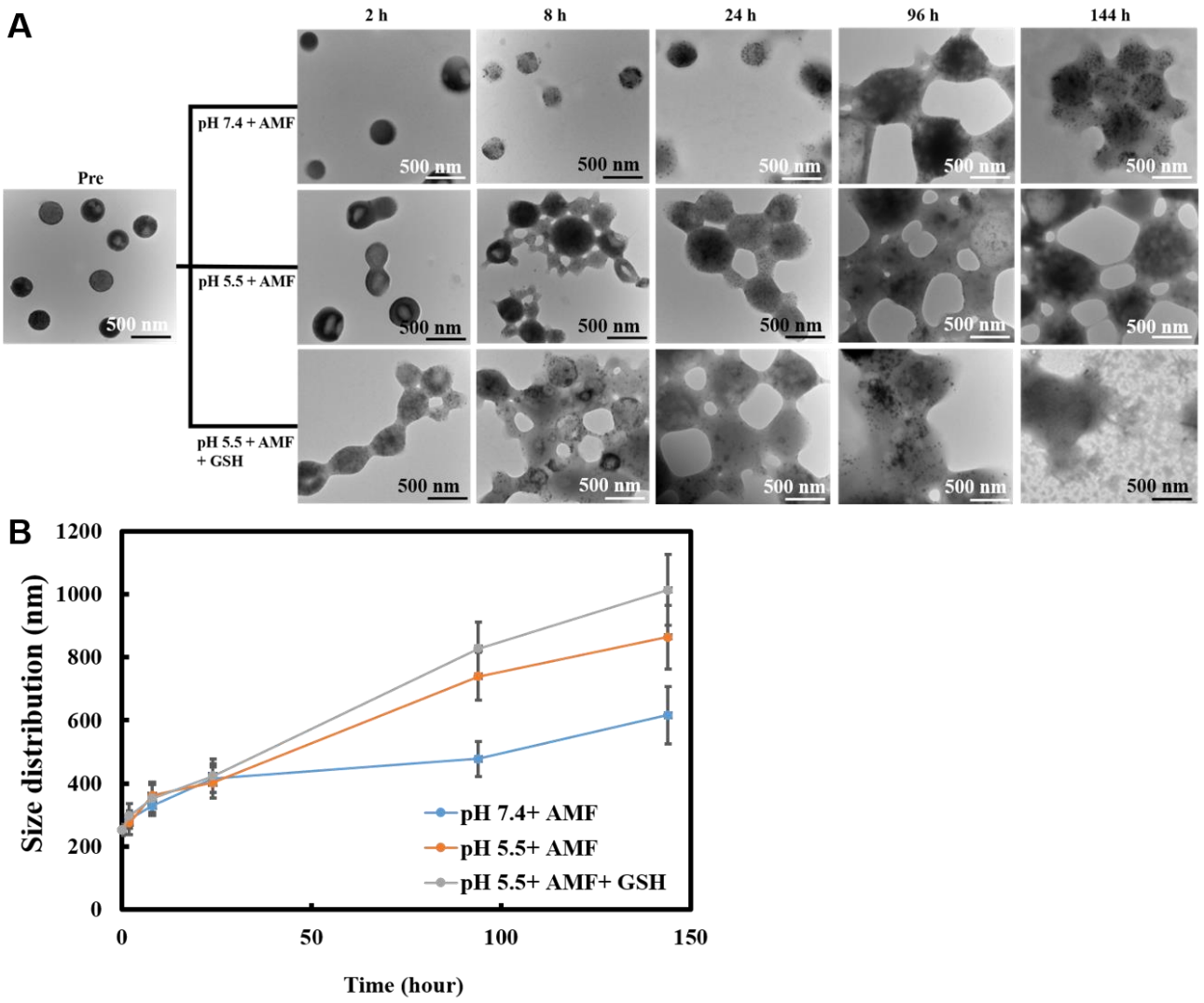

Supplementary Figure S7. Thermal stability test of PSPps-IONPs@DOX NPs with AMF. (A) TEM image changes of IONPs-PSPps@DOX NPs with time. **(B)** Size changes of IONPs-PSPps@DOX NPs with time estimated from **Figure (A)**. IONPs-PSPps@DOX NPs were dispersed in PBS at pH 7.4, pH 5.5, or pH 5.5 containing 5 mM glutathione (GSH) followed by AMF at 10 kW for 15 min, and then placed in a 37 ℃ incubator for various time points. All experiments were performed in triplicate (*n*=3).

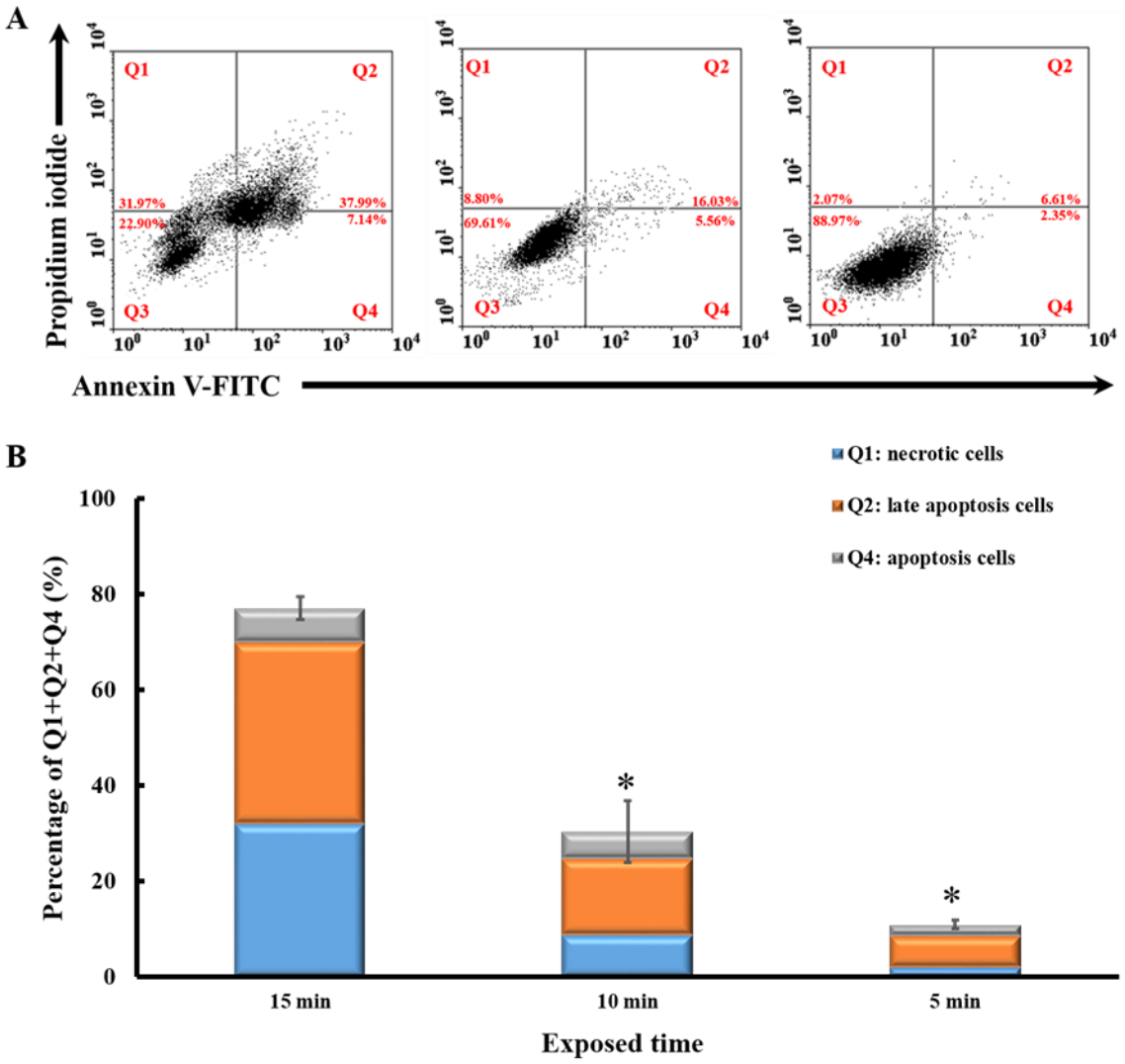

Supplementary Figure S8. Impact of AMF exposure time on cell apoptosis. (A) Annexin-V/PI (propidium iodide) dual-staining assay by flow cytometry. **(B)** The sum of Q1, Q2 and Q3 accounted for the percentage of the death cells. A549 cells were used as a model. Cells were exposed to IONPs-PSPps NPs at 100 μg·mL^{-1} and exposed to AMF at 10 kW for various time points. The four quadrants from Q1 to Q4 corresponded to necrotic cells, late apoptotic cells, viable cells, and apoptotic cells, respectively. Experiments were performed in quadruplicate (n=4, *P<0.05, compared with 15 min).

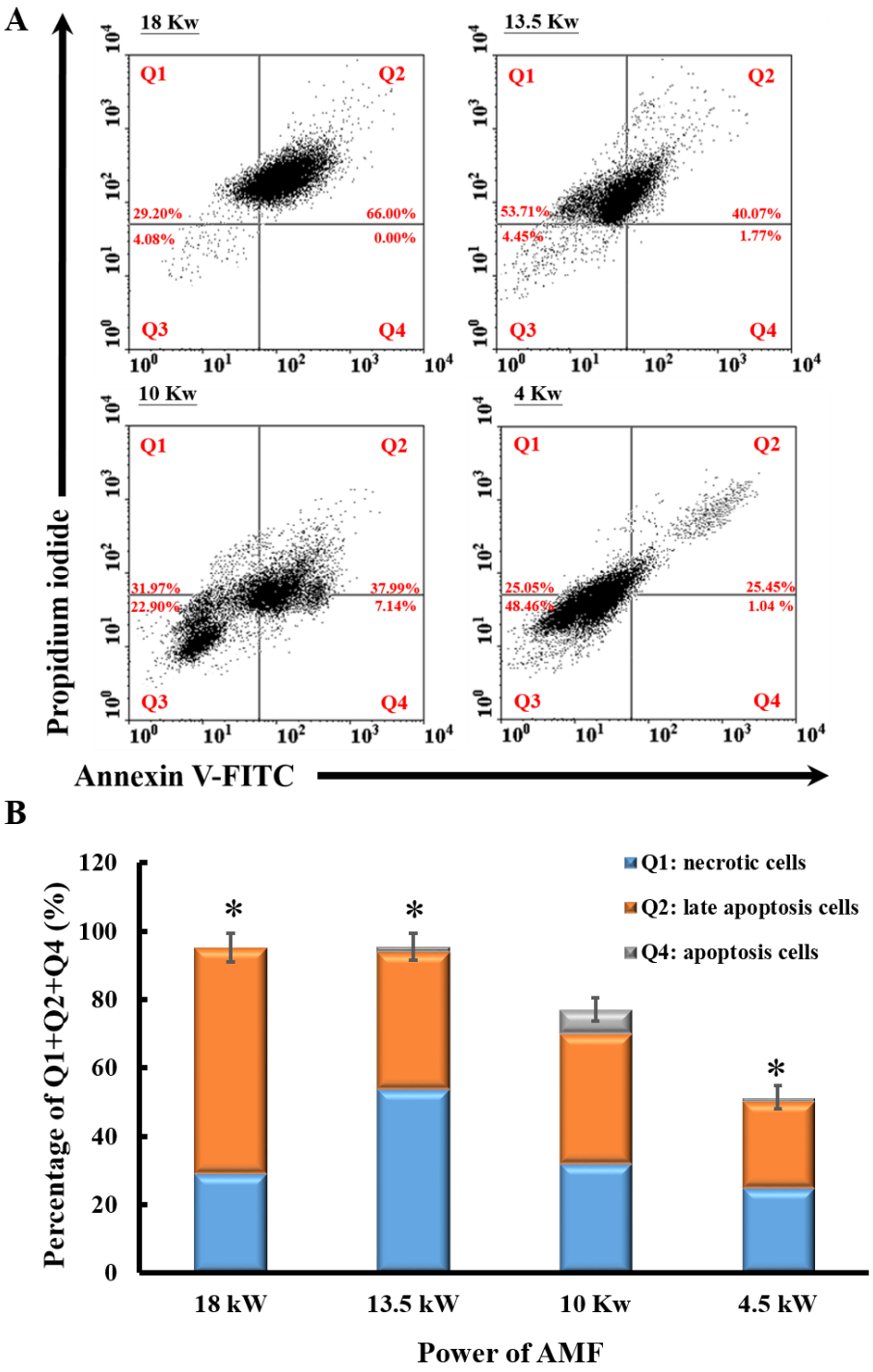

Supplementary Figure S9. Impact of the alternating magnetic field (AMF) power on cell apoptosis. **(A)** Annexin-V/PI (propidium iodide) dual-staining assay by flow cytometry. **(B)** The sum of Q1, Q2 and Q3 accounted for the percentage of the death cells. A549 cells were used as a cell model. Cells were exposed to IONPs-PSPps at 100 μg·mL^{-1} and exposed to AMF at various powers for 15 min. The four quadrants from Q1 to Q4 corresponded to necrotic cells, late apoptotic cells, viable cells, and apoptotic cells, respectively. Experiments were performed in quadruplicate (n=4, *P<0.05, compared with 10 Kw).

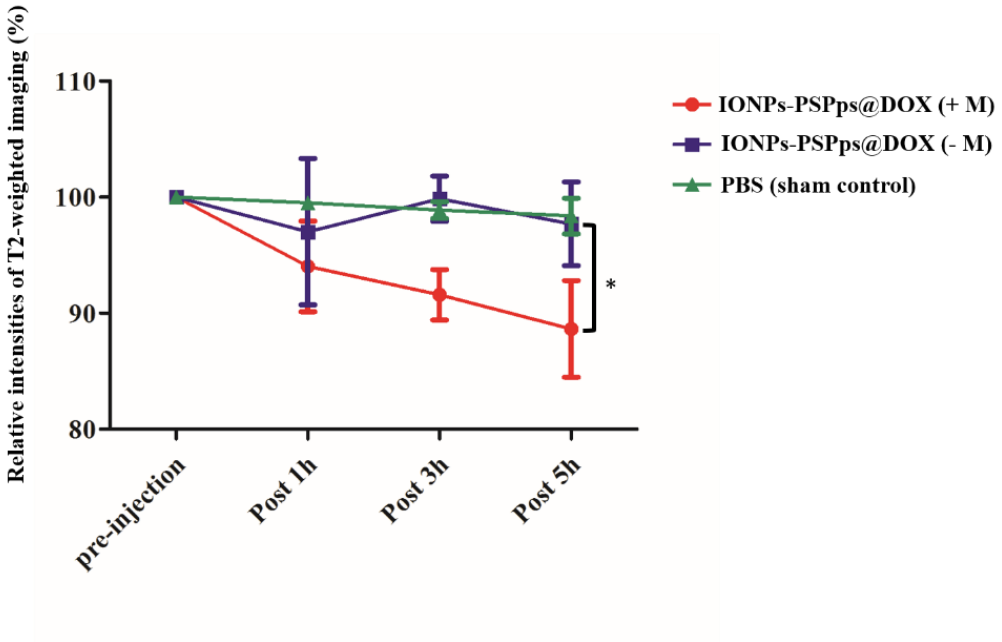

Supplementary Figure S10. *In vivo* MRI contrast. Relative contrast intensities in *in vivo* T_2-weighted images of mice dorsal flank tumors shown in Figure 6A with (+M) or without (-M) assistance from a magnet using a 9.4-T animal MRI system. Mice were injected with IONPs-PSPps@DOX NPs in PBS via the tail vein at a dose of 10 $mg \cdot kg^{-1}$. MRI images were captured at pre-injection and 1, 3, and 5h post-injection of the particles and the relative intensities of T_2-weighted images were calculated using ImageJ software (n=3, *p<0.05).

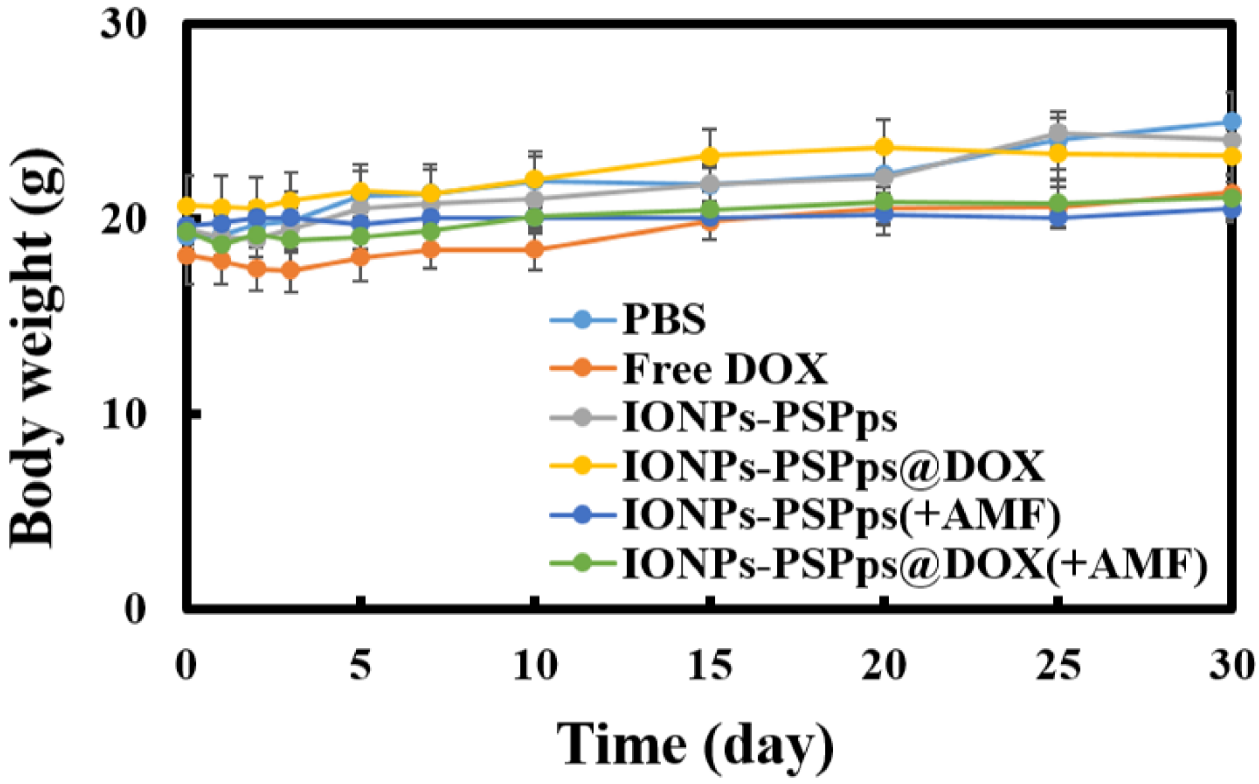

Supplementary Figure S11. Body weight changes of A549-tumor-bearing mice. The body weights of mice in all groups were measured with different time points. Mice were treated with IONPs-PSPps NPs or IONPs-PSPps@DOX NPs, and one of the tumors received assistance from a magnet for 30 min, and subsequently, exposure with (+AMF) at 10 kW for 15 min.

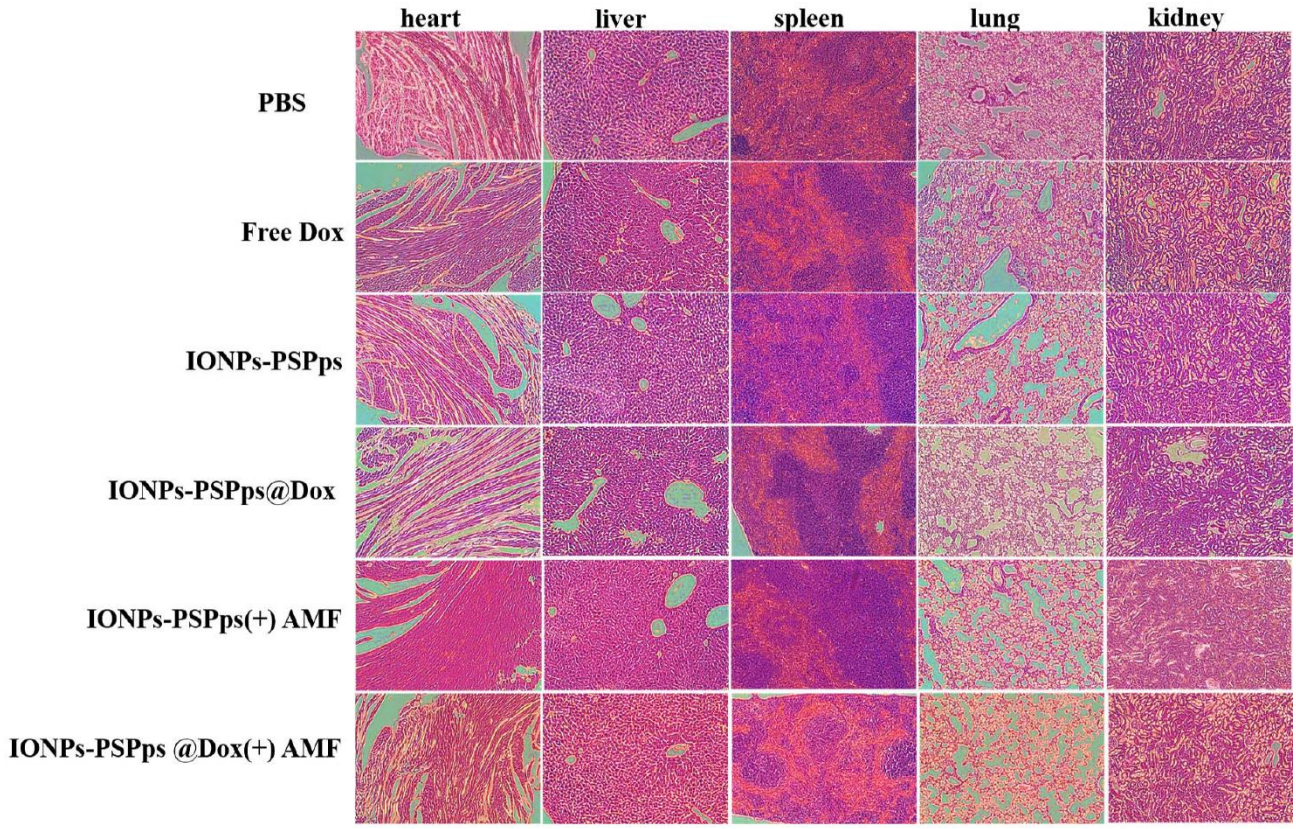

Supplementary Figure S12. Histological staining of the mouse organs. Histological images of the dissected tissues from mice with different treatments stained with hematoxylin and eosin.

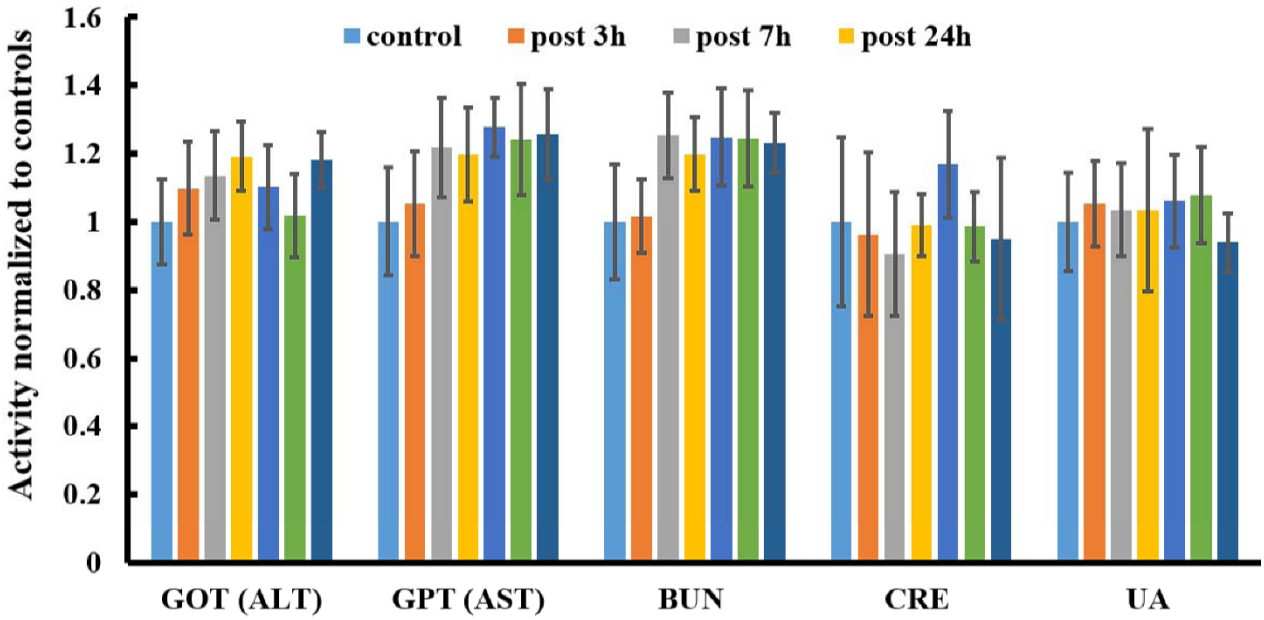

Supplementary Figure S13. Evaluation of Toxicology. The blood biochemical analysis of liver (glutamate oxaloacetate transaminase [GOT] and glutamic-pyruvic transaminase [GPT]) and kidney (blood urea nitrogen [BUN], creatinine [CRE], and uric acid [UA]) in mice treated with IONPs-PSPps@DOX NPs for different time points. Mice were injected with IONPs-PSPps@DOX NPs in PBS via the tail vein at a dose of 24 $mg \cdot kg^{-1}$. Control mice were injected with PBS alone. All the blood biochemical analysis was normalized to the control group (n=3). ALT, alanine aminotransferase; AST, aspartate aminotransferase.